European Polymer Journal 134 (2020) 109805

Contents lists available at ScienceDirect

European Polymer Journal

journal homepage: www.elsevier.com/locate/europolj

Eugenol-derived reconfigurable high-performance epoxy resin for self-deployable smart 3D structures

Jia-Tao Miao[a,*], Meiying Ge[a], Yadong Wu[a,b], Tsung Yu Chou[a], Haopeng Wang[a], Longhui Zheng[a,c], Lixin Wu[a,*]

[a] CAS Key Laboratory of Design and Assembly of Functional Nanostructures, Fujian Key Laboratory of Nanomaterials, Fujian Institute of Research on the Structure of Matter, Chinese Academy of Sciences, Fuzhou 350002, PR China
[b] University of Chinese Academy of Sciences, Beijing 100049, PR China
[c] Fujian Universities and Colleges Engineering Research Center of Soft Plastic Packaging Technology for Food, Fuzhou 350300, PR China

ARTICLE INFO

Keywords:
Biobased epoxy
High performance
Reconfigurability
Self-deploy
3D smart structure

ABSTRACT

Fabricating biobased reconfigurable high performance epoxy resins for self-deployable 3D smart structures is an interesting issue with great challenge. Herein, a biobased trifunctional epoxy monomer (tris(2-methoxy-4-(oxiran-2-ylmethyl)phenyl) phosphate, TMOPP) was derived from eugenol and cured by 4,4′-dithiodianiline (DTDA) to form the dynamic cross-linked TMOPP/DTDA resin. The integrated properties including thermal, mechanical and flame retardancy of TMOPP/DTDA resin are studied systemically. Compared with commercial epoxy resin (diglycidyl ether of bisphenol A (DGEBA)/DTDA), TMOPP/DTDA resin has higher glass transition temperature (217 °C) and tensile strength (95.2 MPa), while these properties are superior to those of biobased dynamic cross-linked epoxy resins reported in literatures. TMOPP/DTDA resin also shows excellent flame retardancy with UL-94 V-0 rating. The trifunctional aromatic structure of TMOPP and the compact cross-linked structure of TMOPP/DTDA resin play a principle role in the outstanding performances. At the same time, permanent shape reconfigurability and self-deployable ability of TMOPP/DTDA resin was exhibited by the transformation from planar film into a 3D "rocking chair" structure. These results provide a new method to produce biobased reconfigurable high performance epoxy resin in a simple and sustainable way, while expand the application of dynamic cross-linked epoxy resins in self-deployable 3D smart structures.

1. Introduction

Three-dimensional (3D) structures have tremendous demands with their extensive application from the daily use to high-edge fields. The production of 3D objects usually depends on molding or 3D printing [1], both of which cost a lot in equipment and need a long time to process the complex or large structures [2,3]. Compared with 3D shapes, two-dimensional (2D) polymer sheets are easier to produce, storage and transport, but the application fields of plane shapes are limited [4]. Combining the advantages of 2D and 3D structures to produce objects by thermosets in a simple way is a great challenge. In addition, the rapid developments of aerospace and electronic information raise high requirements for smart 3D structures with self-deployable ability [5,6].

The geometry of thermosets can be changed by external force to different extend according to their own properties. However, most thermosets show the shape memory behaviors [7], so the permanent shapes of them are difficult to deform. Specifically, shapes of thermosets just can be changed and fixed temporarily, once stimulated by external factors such as heat, electricity, light, and so on [8], the temporary shapes will recover to the original ones and lose the ability to maintain their functions. The nature behind is the permanent cross-linking structures of thermosets which restrict the topological variation, and the internal stress will bring the networks to the original state as well as the macroscopic shapes [9]. To realize the permanent reconfiguration of thermosets, dynamic covalent bonds have been introduced into thermosets including epoxy resins [10–12], thermoset polyurethane [13–15], polyimine [16], acrylate [17], cross-linked poly (caprolactone) [18], furan/maleimide adducts [19], and silyl ether networks [20].

Epoxy resin obtains excellent mechanical properties and heat resistance, so it is one of the most-used polymers occupying 70% market of the thermosets [21–23]. Commercial epoxy resins are usually derived from petroleum resources, so the huge amount utilization of them will

* Corresponding authors.
E-mail addresses: jiataomiao@outlook.com (J.-T. Miao), lxwu@fjirsm.ac.cn (L. Wu).

https://doi.org/10.1016/j.eurpolymj.2020.109805
Received 11 April 2020; Received in revised form 25 May 2020; Accepted 26 May 2020
Available online 27 May 2020
0014-3057/ © 2020 Elsevier Ltd. All rights reserved.

exacerbate the petrochemical resource crisis [24,25]. In addition, 90% of commercial epoxy resins are bisphenol A type epoxy resin, but bisphenol A has been demonstrated to threat human health especially the reproductive capacity [26,27]. Therefore, bisphenol A free epoxy resins are urgently in need.

Non-toxic, renewable and abundant biomass is an emerging considerable candidate for petrochemical resource [28,29]. It could provide various active groups to meet different demands, attracting great attention from scientific and industrial fields in recent years [30–32]. Some biobased dynamic covalent epoxy resins have been reported. Zhang et al. [11] reported repairing and shape changing biobased eugenol epoxy resins (Eu-EP) cured with succinic anhydride. Glass transition temperature (T_g) of these resins ranged from 53 to 58 °C. They also reported a biobased triepoxy (TEP) based on lignin-derived vanillin and guaiacol cured with an anhydride curing agent [33]. T_g of these resins raised to 157–187 °C and tensile strength of them were 62.8–69.2 MPa. These two works formed dynamic cross-linking *via* transesterification, which could occur usually in the presence of catalyst. Wang et al. [34] reported a biobased vitrimer constructed from isosorbide-derived epoxy and aromatic diamines containing disulfide bonds. T_g and tensile strength of this resin was 41.4 °C and 10.98 MPa. Abu-Omar et al. [35] and Feng et al. [36] reported a same epoxy monomer GE-VAN-AP based on vanillin, but cross-linked by Jeffamine and aromatic diamine, respectively. The former recyclable and malleable resin exhibited tensile strength of 46 MPa and T_g of 71 °C, while the latter one had excellent controlled degradability and antibacterial properties with tensile strength of 93 MPa and T_g of 196 °C. Zhu et al. [37] reported a Schiff base epoxy thermoset from vanillin *via* in situ formation of the Schiff base structure and epoxy network. The thermoset possessed a T_g of 172 °C and a tensile strength of 81 MPa. All these works proved the possibilities of fabricating dynamic covalent epoxy resins while the thermal and mechanical properties of biobased dynamic covalent epoxy resins shall be improved and their shape reconfiguration and self-deploy behaviors need to be further studied. In addition, since epoxy resins possess high flammability [38], their applications in advanced areas are seriously limited.

In this paper, a novel biobased dynamic covalent epoxy resin with high performance was designed. Specifically, a trifunctional eugenol-based epoxy monomer with a renewable carbon content as high as 100% was cured by a disulfide-containing hardener to fabricate dynamic cross-linked networks. The integrated performance including thermal, mechanical properties, flame retardancy, shape reconfiguration and self-deployable behaviors and the origin behind were studied systematically.

2. Experimental

2.1. Materials

4,4′-Dithiodianiline (DTDA, Scheme 1) and eugenol were purchased from Energy Chemical, China. Diglycidyl ether of bisphenol A (DGEBA, NPEL 128, with an epoxide equivalent weight of 184–190 g equiv^{-1}) was obtained from Nanya Electronic Materials (Kunshan) Co., Ltd. Tris (2-methoxy-4-(oxiran-2-ylmethyl)phenyl) phosphate (TMOPP) was synthesized from renewable eugenol by ourselves [39].

2.2. Preparation of epoxy resins

TMOPP or DGEBA was blended with DTDA (the molar ratio of epoxy groups to N-H was 1: 1) and stirred at 80 °C for 15 min to get the clear prepolymers. The obtained prepolymers were then poured into a preheated mold. After degassed at 80 °C for 20 min, the mixture was cured at 140 °C for 2 h, 170 °C for 2 h and 200 °C for 2 h. After natural cooling, the cured TMOPP/DTDA or DGEBA/DTDA resins were obtained.

2.3. Characterizations

Differential scanning calorimetry (DSC) spectra were collected by DSC 200 (Netzsch, Germany) under nitrogen atmosphere (60 mL min^{-1}). The monomers were tested from 30 to 120 °C with a heating rate of 10 °C min^{-1} to record the melt process. The prepolymers were tested from 30 to 280 °C with a heating rate of 5, 10, 15, 20 °C min^{-1}.

Thermogravimetric analyzer (TGA) tests were performed by an STA449F3 apparatus (Netzsch, Germany) under nitrogen or air atmosphere at a flow rate of 20 mL min^{-1}. The temperature tested ranged from 30 to 800 °C with a heating rate of 10 °C min^{-1}.

Dynamic mechanical analyses (DMA) were conducted on TA DMA Q800 apparatus (USA). A film tension clamp was used and the dimensions of the specimens were (30 ± 0.02) mm × (3 ± 0.02) mm × (1 ± 0.02) mm. The experiments were carried out in "multi-frequency strain" mode at a frequency of 1.0 Hz and deflection amplitude of oscillation 10 μm. Samples were heated by 3 °C min^{-1} from 25 °C to 250 °C. Cross-linking density (υ_e) of thermosetting resins can be calculated by the classical rubbery elasticity theory using Eq. (1).

$$E' = 3\upsilon_e RT \quad (1)$$

where E' is the minimum storage modulus in the rubbery plateau region; T is the corresponding temperature; and R is the universal constant (8.314 J mol^{-1} K^{-1}) [40].

Stress relaxation behaviors were tested on TA DMA Q800 apparatus (USA) in "stress relaxation" mode with a film tension clamp. The dimensions of the specimens were (30 ± 0.02) mm × (3 ± 0.02) mm × (1 ± 0.02) mm. The tests were conducted at 200, 210, 220, 230 °C, respectively, under the constant strain of 1.5%.

Reconfiguration was tested on TA DMA Q800 apparatus (USA) in "strain rate" mode with a film tension clamp at 230 °C. The sample was stretched under external force to the predetermined strain of 2% and 4%. The reconfigurable shape retention ratio (R_{ret}) was calculated by Eq. (2) [18].

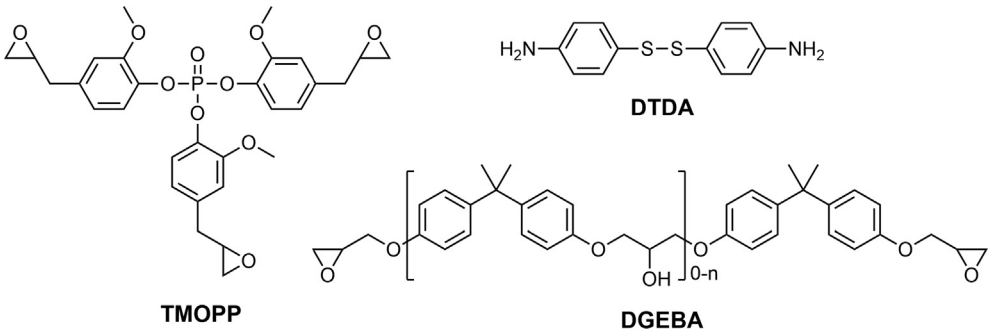

Scheme 1. Chemical structures of biobased epoxy monomer TMOPP, DGEBA and curing agent (DTDA).

$$R_{ret} = \frac{\varepsilon_{plasticity}}{\varepsilon_{force}} \times 100\% \quad (2)$$

where $\varepsilon_{plasticity}$ is the final strain recorded and ε_{force} is the strain under external force.

The micromechanical properties of the materials were measured by a nanoindenter instrument (Tribo Indenter 750, Hysitron Inc., USA). A Berkovich diamond indenter with a probe of 50 nm in radius was employed. Samples were tested in a typical load–hold–unload pattern. The loading and unloaded speeds were 1600 μN S^{-1}. The maximum indentation force was set to be 8000 μN and kept for 2 s. The hardness (H) was calculated using Eq. (3) according to the Oliver–Pharr method [41].

$$H = \frac{P_{max}}{A_c} \quad (3)$$

where P_{max} is the maximum applied load, A_c is the contact area between the sample and intender.

Measurement of the Young's modulus (E) follows from its relationship to contact area and the measured unloading stiffness through Eq. (4)

$$S = \beta \frac{2}{\sqrt{\pi}} E_{eff} \sqrt{A} \quad (4)$$

where E_{eff} is the effective Young's modulus defined by Eq. (5)

$$\frac{1}{E_{eff}} = \frac{1 - \nu^2}{E} + \frac{1 - \nu_i^2}{E_i} \quad (5)$$

where ν is the Poisson's ratio of the sample and E_i, ν_i are Young's modulus and Poisson's ratio of the indenter, respectively.

Tensile properties and stress-strain curves of resins were obtained by a universal material test machine (AGX-100 plus, Shimadzu, Japan) according to ISO 527-2:2012 standard (specimen type: 1BA) with an extensometer gauge length of 25 mm. The samples were tested at room temperature and the elongation rate of 2 mm min^{-1}. All of final tensile data were the mean value of five effective measurements.

Micro combustion calorimetery (MCC) was performed on a GOVMARK MCC-2 instrument (USA). 5 mg samples were heated from 150 to 750 °C at a heating rate of 60 °C min^{-1} under air atmosphere. MCC data were the mean value of two effective measurements.

The vertical burning (UL-94) tests were done on a horizontal and vertical burning tester CZF-5 (Nanjing Jiangning Analysis Instrument Co., Ltd., China) according to ASTM D3801-2019; the dimensions of the specimens were (125 ± 0.02) mm × (13 ± 0.02) mm × (1 ± 0.02) mm.

Scanning electron microscope (SEM, Hitachi S-4700, Japan) was used to observe the morphologies of the samples at an accelerating voltage of 15 kV. Adequate electrical conductivity of the surface of sample was achieved through pretreated by vacuum metal spraying technology before the tests.

3. Results and discussion

3.1. Curing behaviors

As shown in Fig. 1(a), both of TMOPP and DTDA monomers had a melting peak since they are solid at room temperature. DSC tests at different heating rate (5, 10, 15, 20 °C min^{-1}) were conducted to study the curing behaviors of TMOPP/DTDA and DGEBA/DTDA prepolymers. As shown in Fig. 1(b), there was no melting process of TMOPP/DTDA prepolymers during the test, and all of DSC curves of the prepolymers exhibited only one curing exothermic peak that related to the reaction between epoxy and amino. The exothermic peak moved to higher temperature with the increase of heating rate (β), and TMOPP/DTDA showed higher exothermic peak under the same β. The relationship between the temperature of curing peak (T_p) and β accords to the

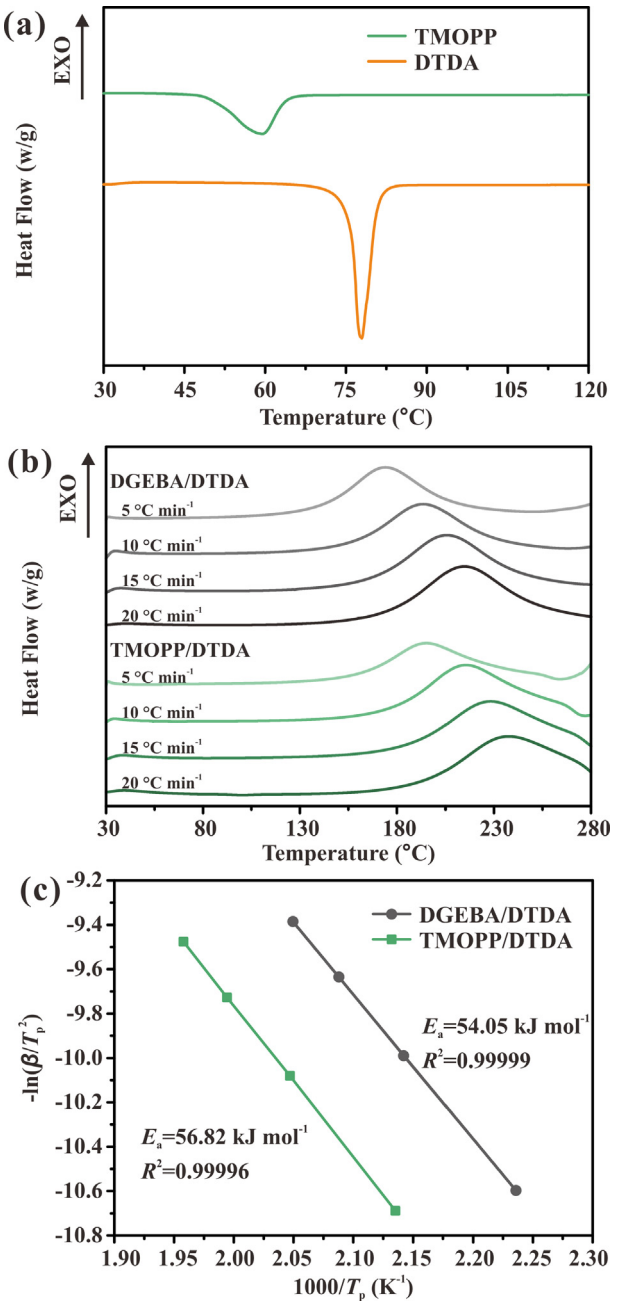

Fig. 1. (a) DSC thermograms of TMOPP and DTDA at heating rate of 10 °C min^{-1}. (b) DSC thermograms of DGEBA/DTDA and TMOPP/DTDA prepolymers at different heating rate (5, 10, 15, 20 °C min^{-1}). (c) Fitting curves of exothermic peak temperature *vs* heating rate of DGEBA/DTDA and TMOPP/DTDA prepolymers.

Kissinger Eq. (6).

$$\ln\left(\frac{\beta}{T_p^2}\right) = \ln\left(\frac{AR}{E_a}\right) - \frac{E_a}{RT_p} \quad (6)$$

where E_a is the reaction activation energy, A is the pre exponential factor and R is the universal constant (8.314 J mol^{-1} K^{-1}). Fig. 1(c) is the fitting curves of ln (β/T_p^2) and $1000/T_p$. The values of E_a calculated from the slope of the curves were 56.3 kJ mol^{-1} of TMOPP/DTDA prepolymer and 54.0 kJ mol^{-1} of DGEBA/DTDA prepolymer. The slight higher E_a of TMOPP/DTDA prepolymer resulted from the trifunctional structure of TMOPP that produced larger steric hindrance during the curing reaction.

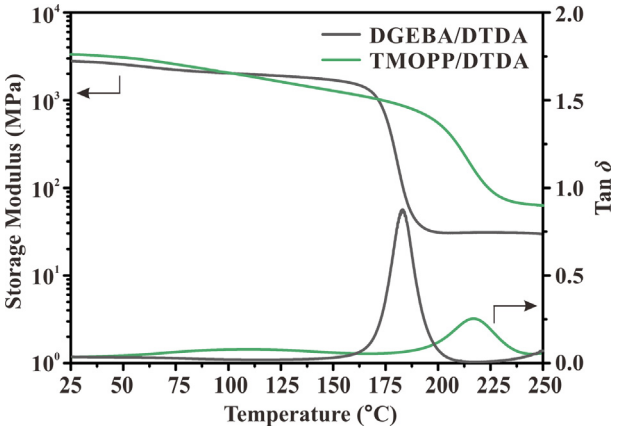

Fig. 2. Storage modulus and tan δ related to temperature for DGEBA/DTDA and TMOPP/DTDA resins.

3.2. Thermal and mechanical properties

DMA is an effective way to evaluate the thermal resistance and cross-linking structures of polymers for its high sensitivity. Usually, the temperature corresponding to the peak of the Tan δ-temperature curves is defined as the T_g. As shown in Fig. 2, both TMOPP/DTDA and DGEBA/DTDA resins had only one peak of the Tan δ-temperature curves, and the storage modulus (E') of them decreased sharply at the corresponding temperature, indicating the obvious glass transition behaviors. T_g of TMOPP/DTDA resin is 217 °C, 34 °C higher than that of DGEBA/DTDA resin. Glass transition is caused by the motion of molecular chains, rigid chain segments and compact networks that go against molecular chain movement will result in a higher T_g value. TMOPP has a trifunctional structure, which restricts the rotation of chemical bonds, making it more rigid than DGEBA. At the same time, the cross-linking densities of TMOPP/DTDA and DGEBA/DTDA resins are calculated to be 4870 and 2487 mol m^{-3}, respectively. More cross-linking points lead to the higher cross-linking density of TMOPP/DTDA resin, contributing to the higher T_g value. T_g is the upper boundary on thermosetting resins utilization, so TMOPP/DTDA resin is expected to be applied in harsher environments. E' values of TMOPP/DTDA and DGEBA/DTDA resins at 25 °C, reflecting the stiffness of the cured resins, are 3340 MPa and 2802 MPa, respectively. The high stiffness of TMOPP/DTDA resin also resulted from the rigid molecular structure and highly cross-linked networks.

Nanoindentation is a considerable method to measure micro-mechanical properties of resins in nano-scale with only a little patch of sample and the results obtained are more accurate. The typical indentation load-displacement curves of TMOPP/DTDA and DGEBA/DTDA resins were shown in Fig. 3(a). With the load increases, the displacement advanced gradually. The elastic deformation firstly rose, following by plastic deformation, and finally the peak displacement (h_{max}) is reached under the peak load. During unloading process, elastic deformation recovered, showing the decreased displacement. When load is released completely, there was still displacement left, this is because of the plastic deformation which cannot be restored and will cause an indentation on the sample surface. TMOPP/DTDA resin had a smaller h_{max} under the same peak load of 8000 μN, indicating a stronger resistance to the indenter penetration. Young's modulus (E), hardness (H) can be calculated from the unloading section of the displacement–load curves. As shown in Fig. 3(b), E and H values of TMOPP/DTDA resin are 7.31 GPa and 0.75 GPa, surpassing those values of DGEBA/DTDA resin. The rigid structure of TMOPP and high cross-linking density of TMOPP/DTDA resin improved the hardness of the cured resins.

Both of TMOPP/DTDA and DGEBA/DTDA resins exhibited typical stress-strain curves for rigid materials (Fig. 4). The tensile properties

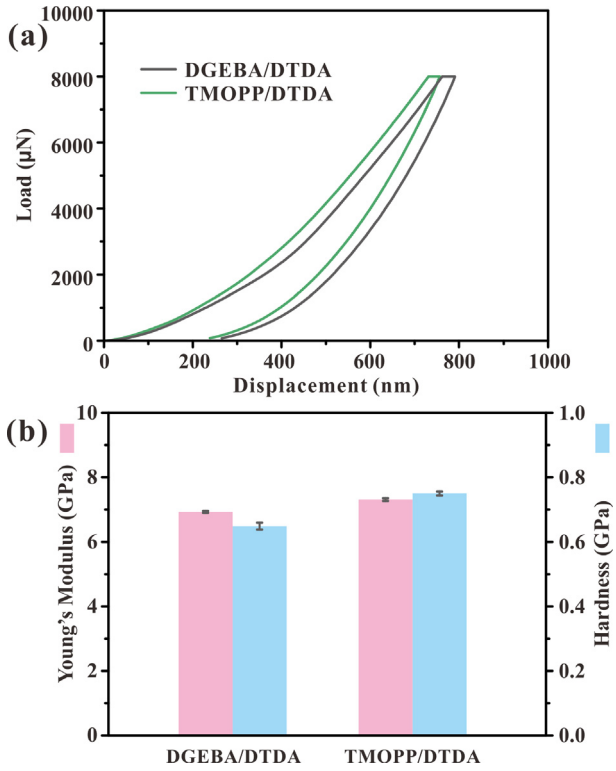

Fig. 3. (a) Representative load–displacement curves of DGEBA/DTDA and TMOPP/DTDA resins with a maximum load of 8000 μN. The loading, unloading rate and holding time at peak load are 1600 μN S^{-1}, 1600 μN S^{-1} and 2 s, respectively. (b) The hardness (H) and Young's modulus (E) of DGEBA/DTDA and TMOPP/DTDA resins calculated from the obtained load–displacement curves.

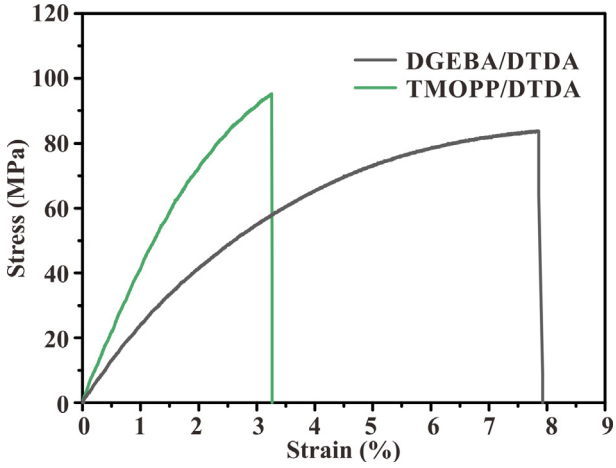

Fig. 4. Tensile stress–strain curves of DGEBA/DTDA and TMOPP/DTDA resins.

Table 1
Tensile properties of DGEBA/DTDA and TMOPP/DTDA resins.

Resin	σ_b (MPa)	E_t (MPa)	ε_b (%)
TMOPP/DTDA	95.2 ± 2.1	4145 ± 105	3.3 ± 0.4
DGEBA/DTDA	84.3 ± 1.4	2554 ± 42	7.5 ± 0.6

including tensile strength (σ_b), tensile modulus (E_t) and elongation at break (ε_b) are listed in Table 1. TMOPP/DTDA resin possesses a 12.9% higher tensile strength value and 62.3% higher tensile modulus value, but a lower elongation at break value than those of DGEBA/DTDA resin. The higher modulus and strength is owing to the more rigid cross-

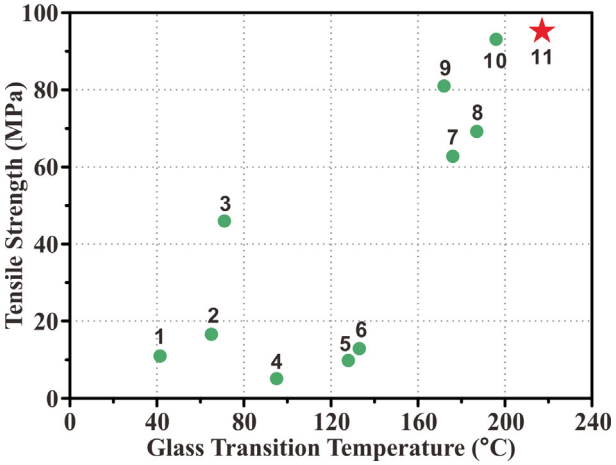

Fig. 5. A comparison of the tensile strength and T_g of biobased epoxy resins containing dynamic covalent bonds reported in literature and this work (11). 1: MDS-EPO [34], 2: ESO-FPA,[42] 3: EN-VAN-AP [35], 4: Se-EP/Oz-L 1:0.75 [43], 5: Se-EP/Oz-L 1:1 [43], 6: Se-EP/Oz-L 1:1.5 [43], 7: TEP-2 [33], 8: TEP-1 [33], 9: MB-PACM [37], 10: VBE-DDM [36].

linking networks of TMOPP/DTDA resin formed by trifunctional structure of TMOPP, as well as the higher cross-linking density of the cross-linking networks.

In order to illustrate the excellent thermal and mechanical properties of TMOPP/DTDA resin more intuitively, a comparison of the tensile strength and T_g of biobased epoxy resins containing dynamic covalent bonds reported in literature and this work are shown in Fig. 5. Tensile strength of these literature-reported resins range from 5.1 to 93 MPa while T_g of them are in the range of 41.4–196 °C. The red star represents for TMOPP/DTDA resin located in the upper right corner with a tensile strength higher than 95 MPa and a T_g over 200 °C. It is obvious that TMOPP/DTDA resin obtains better thermal and mechanical properties than all of these resins, which is benefit for expanding the application fields of biobased dynamic cross-linked epoxy resins into more difficult conditions.

3.3. Thermal stability

TGA was taken to test the initial thermal decomposition temperature (T_{di}) that is defined as the temperature at which resin lose 5% of their weight. Fig. 6 shows the TGA curves of TMOPP/DTDA and DGEBA/DTDA resins under N_2 and air atmosphere. Under N_2 atmosphere, only the decomposition of the polymer networks can be observed. TMOPP/DTDA resin achieved T_{di} (299 °C) and the peak temperature of decomposition (T_{max}, 311 °C) earlier than DGEBA/DTDA resin. Since the bond energy of P-O bond is lower than C-C bond, it will break at lower temperature, resulting in a lower T_{di} and T_{max}. However, TMOPP/DTDA resin decomposed more gently after T_{max}, and remained larger char yield (48.5% *vs* 19.0%) at 800 °C. The TGA curves of TMOPP/DTDA and DGEBA/DTDA resins under air atmosphere displayed two stages. The first stage related to the decomposition of the polymer networks, while the second one is the pyrolysis of the carbon residue. T_{max} of the carbon residue of TMOPP/DTDA resin is 764 °C, much higher than that of DGEBA/DTDA resin (580 °C), indicating that the carbon residue of TMOPP/DTDA resin was more stable. The larger amount and denser carbon residue indicated that TMOPP/DTDA resin has better flame retardancy than DGEBA/DTDA resin, which will be further confirmed by the following MCC and UL-94 tests.

3.4. Flame retardancy

MCC is used to assess the flammability of materials which can quickly acquire the combustion parameters with only a small amount

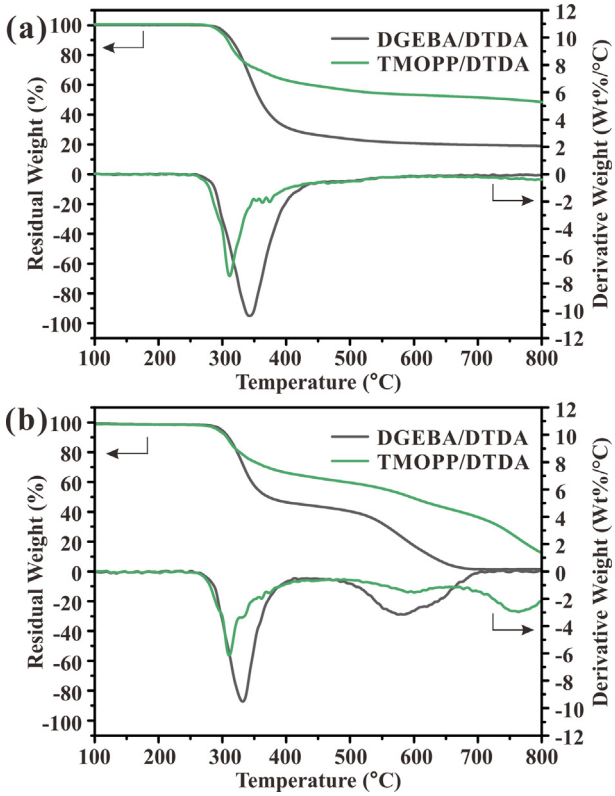

Fig. 6. TG and DTG curves of DGEBA/DTDA and TMOPP/DTDA resins under N_2 (a) and air (b) atmosphere.

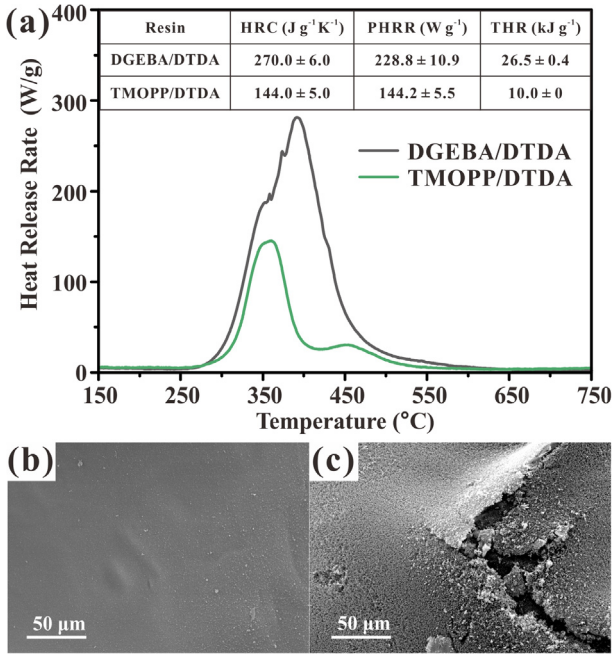

Resin	HRC (J g^{-1}K^{-1})	PHRR (W g^{-1})	THR (kJ g^{-1})
DGEBA/DTDA	270.0 ± 6.0	228.8 ± 10.9	26.5 ± 0.4
TMOPP/DTDA	144.0 ± 5.0	144.2 ± 5.5	10.0 ± 0

Fig. 7. (a) Heat release rate-time curves from MCC tests of DGEBA/DTDA and TMOPP/DTDA resins. SEM micrographs of char surfaces of TMOPP/DTDA resin (b) and DGEBA/DTDA resin (c) after UL-94 tests.

(approximately 5 mg) of samples. The heat release rate (HRR) - temperature curves and the corresponding parameters including heat release capacity (HRC), peak heat release rate (PHRR) and total heat release (THR) are shown in Fig. 7(a). It is obvious that the heat release progress of TMOPP/DTDA resin was gentler than DGEBA/DTDA resin, which is consentient with the results from TGA. In addition, HRC, PHRR

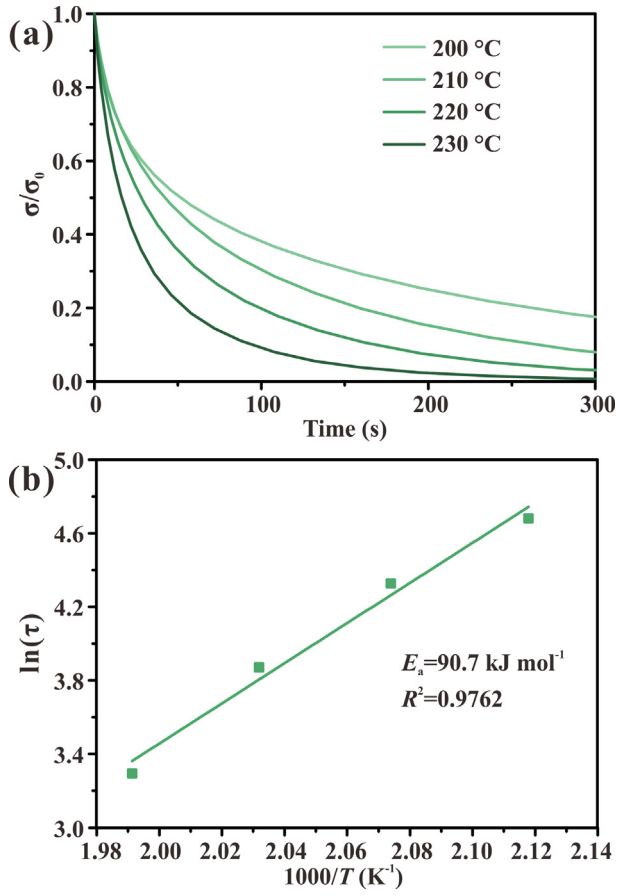

Fig. 8. (a) Stress relaxation curves of TMOPP/DTDA resin at different temperatures. (b) Fitting of the relaxation times to temperatures according to Arrhenius' equation of TMOPP/DTDA resin.

and THR values of TMOPP/DTDA resin were 144 ± 5 J g^{-1} K^{-1}, 144.2 ± 5.5 W g^{-1}, 10.0 ± 0 kJ g^{-1}, 46.7%, 37.0% and 62.3%, respectively, lower than those of DGEBA/DTDA resin. Vertical burning test was conducted to characterize the ability of resins to extinguish flame. DGEBA/DTDA resin showed UL-94 no rating while TMOPP/DTDA resin achieved the highest UL-94 V0 rating, indicating that TMOPP/DTDA resin could better prevent flame from spreading. Above results demonstrate that TMOPP/DTDA resin obtains much better flame retardancy than DGEBA/DTDA resin. SEM has been used to observe the morphology of char surfaces of DGEBA/DTDA and TMOPP/DTDA resins after UL-94 tests. As shown in Fig. 7(b) and (c), the char surfaces of TMOPP/DTDA resin was condensed and continuous while that of DGEBA/DTDA resin was loose with crack. Compared to DGEBA/DTDA resin, the char residue of TMOPP/DTDA resin could better prevent fire from spreading during the combustion, thus endowing TMOPP/DTDA resin with better flame retardancy.

3.5. Reconfiguration and self-deploy behaviors

The addition of disulfide bonds can fabricate dynamic cross-link in thermosetting resins [44], thus the stress relaxation will be achieved. Fig. 8(a) shows the normalized stress relaxation curves of TMOPP/DTDA resin at 200, 210, 220 and 230 °C. With the temperature increased, the relaxation rate and the final relaxation degree were increasing. The relaxation time (τ), defined as the time when stress release to 1/e of its original value, of TMOPP/DTDA resin ranged from 109 s at 200 °C to 27 s at 230 °C. Moreover, the stress of TMOPP/DTDA resin almost completely relaxed at 230 °C after 300 s. This is because the exchange of disulfide bonds was accelerated and the chain segments slip was easier and quicker at high temperature. The disulfide bonds exchange was quantified by activation energy (E_a) which can be obtained through linear fitting of ln (τ) with 1000/T according to Arrhenius' law (Eq. (7)).

$$\ln(\tau) = \ln(\tau_0) + \frac{E_a}{RT} \tag{7}$$

As shown in Fig. 8(b), τ values of TMOPP/DTDA resin conformed to Arrhenius' law and the E_a was calculated to be 90.7 kJ mol^{-1}. Another crucial characteristic value is the topology freezing transition temperature (T_v), relating to the temperature at which the topological structures of networks changes and transform from solid to liquid state by dynamic bonds exchange. T_v is conventionally obtained from eqn (7) *via* τ* value chosen as the time when the viscosity (η) reaches 10^{12} Pa s. The τ* value can be got from Eqs. (8) and (9)

$$\eta = G * \tau^* \tag{8}$$

$$G = E'/2(1+\nu) \approx E'/3 \tag{9}$$

where E' is the storage modulus at rubbery state obtained from DMA.

The T_v of TMOPP/DTDA resin was calculated to be 101.3 °C, 116 °C lower than its T_g. For thermosetting resins, the chain segments motion will not be activated until the temperature achieves T_g. Therefore, although T_v is below T_g, the networks are still frozen until heated to T_g.

Since the topologic structures of TMOPP/DTDA resin can be reconfigured, they exhibit different behaviors with traditional thermosets at higher temperature. Fig. 9(a) shows the strain and stress *vs* time curves of TMOPP/DTDA resin at 230 °C. At the first process, the sample was stretched by 2% deformation and kept for 15 min to undergo the reconfiguration process. And then, the force was unloaded, the strain of TMOPP/DTDA resin did not recover to 0 but still remained 92.9%. The sample was then stretched to 4% deformation to start the second reconfiguration process. After 15 min, 87.4% strain was remained. During both processes, stress of the sample reached its peak value once the predetermined deformation was arrived and then stress relaxation started. The reconfiguration of TMOPP/DTDA resin mainly depends on the exchange of disulfide bonds which is shown in Fig. 9(b). To be specific, when loaded external force and deformed at 230 °C, the motion of the segments was activated and disulfide bonds in the networks began to exchange to release the stress. During this process, the topologic structures of the networks were changed as well as the macroscopical permanent shape of the sample. Therefore, when the external force was removed, shape of the sample would not recover to the origin one. Fig. 9(c) is an example of reconfiguration of TMOPP/DTDA resin. The first planar permanent shape I was deformed and reconfigured at 230 °C for 30 min to obtain the second 3D permanent U-shape. Cooled to room temperature, the U-shape was demonstrated to be fixed. Then the U-shape was reheated to 230 °C, during which the U-shape did not recover to the first I-shape, indicating that after reconfiguration, the 3D shape obtained was a new permanent shape and free from environment stimulations. Likewise, the U-shape was deformed to M-shape and reconfigured at 230 °C for 30 min. The 3D M-shape was also a new permanent shape. A more complex "rocking chair" object was obtained by the transformation of a planar film and the self-deployable behavior was exhibited. As shown in Fig. 9(d), a planar film was reconfigured at 230 °C for 30 min to form a new permanent "rocking chair" 3D structure through reconfiguration. Then the "rocking chair" was deformed to a planar film for a few seconds at 220 °C under external force and fixed at room temperature. When reheated to 220 °C, the planar structure underwent a self-deploy process to the "rocking chair" object (Movie S1). The self-deploy mainly depend on the shape memory character of the resin. The 2D plane shape was firstly deformed to a complex 3D shape permanently through reconfiguration; and then the 3D shape was fixed to a 2D plane one temporarily under external force; finally, the temporary shape was reheated to recover the 3D shape *via* shape memory behaviors thus realizing the self-deploy process. These results

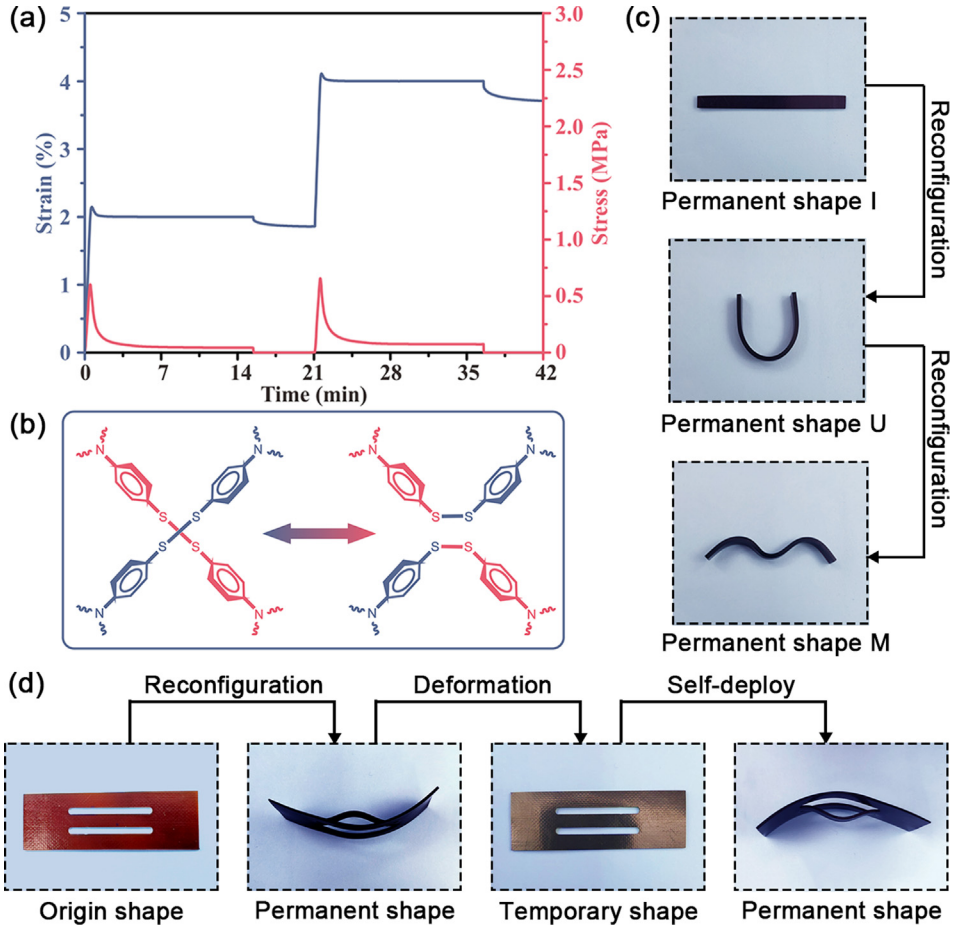

Fig. 9. (a) Consecutive reconfiguration of TMOPP/DTDA resin at 230 °C. (b) Dynamic reversible exchange mechanism of disulfide bonds. (c) Consecutive reconfiguration (from shape I to shape U to shape M) of TMOPP/DTDA resin. (d) Reconfiguration and self-deploy process of TMOPP/DTDA resin.

intuitively proved the reconfigurability of TMOPP/DTDA resin to form 3D objects from 2D plane materials in a simple method and showed the enormous potential of TMOPP/DTDA resin in the application of 3D smart self-deployable structures.

4. Conclusions

Biobased TMOPP/DTDA resin with dynamic disulfide bonds derived from eugenol was fabricated. The trifunctional aromatic structure of TMOPP and the compact cross-linked structures endow the TMOPP/DTDA resin with excellent integrated properties including outstanding thermal, mechanical properties and good flame retardancy. Dynamic exchanges of disulfide bonds make TMOPP/DTDA resin have permanent shape reconfigurability through stress relaxation process. The self-deployable ability was confirmed by a spontaneous deformation from a planar film to a 3D “rocking chair” object. The biobased TMOPP/DTDA resin demonstrates a simple and sustainable way to produce 3D structures and broadens the application fields of biobased dynamic cross-linked epoxy resins especially in 3D smart structures.

CRediT authorship contribution statement

Jia-Tao Miao: Conceptualization, Methodology, Investigation, Writing - review & editing, Funding acquisition. **Meiying Ge:** Formal analysis, Visualization, Writing - original draft. **Yadong Wu:** Validation. **Tsung Yu Chou:** Visualization. **Haopeng Wang:** Investigation. **Longhui Zheng:** Supervision, Project administration. **Lixin Wu:** Resources, Funding acquisition.

Declaration of Competing Interest

The authors declare that they have no known competing financial interests or personal relationships that could have appeared to influence the work reported in this paper.

Acknowledgements

The authors acknowledge the financial support provided by the China Postdoctoral Science Foundation (Grant No.: 2019M662256), the National Key Research and Development Program of China (Grant No.: 2016YFB1100900), the STS Project of Fujian-CAS (Grant No.: 2018T3011, 2019T3016 and 2019T3018), and the Open Project Program of Fujian Universities and Colleges Engineering Research Center of Soft Plastic Packaging Technology for Food.

Appendix A. Supplementary material

Supplementary data to this article can be found online at https://doi.org/10.1016/j.eurpolymj.2020.109805.

References

[1] X. Kuang, D.J. Roach, J. Wu, C.M. Hamel, Z. Ding, T. Wang, M.L. Dunn, H.J. Qi, Advances in 4D printing: materials and applications, Adv. Funct. Mater. 29 (2) (2019) 1805290.
[2] R.R. Kohlmeyer, P.R. Buskohl, J.R. Deneault, M.F. Durstock, R.A. Vaia, J. Chen, Shape-reprogrammable polymers: encoding, erasing, and re-encoding, Adv. Mater. 26 (48) (2014) 8114–8119.
[3] L. Huang, R. Jiang, J. Wu, J. Song, H. Bai, B. Li, Q. Zhao, T. Xie, Ultrafast digital

printing toward 4D shape changing materials, Adv. Mater. 29 (7) (2017) 1605390.
[4] Y. Yang, E.M. Terentjev, Y. Wei, Y. Ji, Solvent-assisted programming of flat polymer sheets into reconfigurable and self-healing 3D structures, Nat. Commun. 9 (1) (2018) 1906.
[5] Y. Liu, J. Genzer, M.D. Dickey, "2D or not 2D": Shape-programming polymer sheets, Prog. Polym. Sci. 52 (2016) 79–106.
[6] S. Felton, M. Tolley, E. Demaine, D. Rus, R. Wood, A method for building self-folding machines, Science 345 (6197) (2014) 644–646.
[7] Q. Zhao, H.J. Qi, T. Xie, Recent progress in shape memory polymer: New behavior, enabling materials, and mechanistic understanding, Prog. Polym. Sci. 49–50 (2015) 79–120.
[8] J. Leng, X. Lan, Y. Liu, S. Du, Shape-memory polymers and their composites: Stimulus methods and applications, Prog. Mater. Sci. 56 (7) (2011) 1077–1135.
[9] W. Zou, J. Dong, Y. Luo, Q. Zhao, T. Xie, Dynamic covalent polymer networks: from old chemistry to modern day innovations, Adv. Mater. 29 (14) (2017) 1606100.
[10] J. Zhu, G. Fang, Z. Cao, X. Meng, H. Ren, A self-folding dynamic covalent shape memory epoxy and its continuous glass fiber composite, Ind. Eng. Chem. Res. 57 (15) (2018) 5276–5281.
[11] T. Liu, C. Hao, L. Wang, Y. Li, W. Liu, J. Xin, J. Zhang, Eugenol-derived biobased epoxy: shape memory, repairing, and recyclability, Macromolecules 50 (21) (2017) 8588–8597.
[12] Z. Yang, Q. Wang, T. Wang, Dual-triggered and thermally reconfigurable shape memory graphene-vitrimer composites, ACS Appl. Mater. Interfaces 8 (33) (2016) 21691–21699.
[13] N. Zheng, Z. Fang, W. Zou, Q. Zhao, T. Xie, Thermoset shape-memory polyurethane with intrinsic plasticity enabled by transcarbamoylation, Angew. Chem. Int. Edit. 55 (38) (2016) 11421–11425.
[14] N. Zheng, J. Hou, Y. Xu, Z. Fang, W. Zou, Q. Zhao, T. Xie, Catalyst-free thermoset polyurethane with permanent shape reconfigurability and highly tunable triple-shape memory performance, ACS Macro Lett. 6 (4) (2017) 326–330.
[15] S. Ji, F. Fan, C. Sun, Y. Yu, H. Xu, Visible light-induced plasticity of shape memory polymers, ACS Appl. Mater. Interfaces 9 (38) (2017) 33169–33175.
[16] S. Wang, S. Ma, Q. Li, W. Yuan, B. Wang, J. Zhu, Robust, fire-safe, monomer-recovery, highly malleable thermosets from renewable bioresources, Macromolecules 51 (20) (2018) 8001–8012.
[17] J.-T. Miao, M. Ge, S. Peng, J. Zhong, Y. Li, Z. Weng, L. Wu, L. Zheng, Dynamic imine bond-based shape memory polymers with permanent shape reconfigurability for 4D printing, ACS Appl. Mater. Interfaces 11 (43) (2019) 40642–40651.
[18] Q. Zhao, W. Zou, Y. Luo, T. Xie, Shape memory polymer network with thermally distinct elasticity and plasticity, Sci. Adv. 2 (1) (2016) e1501297.
[19] G. Zhang, Q. Zhao, L. Yang, W. Zou, X. Xi, T. Xie, Exploring dynamic equilibrium of diels-alder reaction for solid state plasticity in remoldable shape memory polymer network, ACS Macro Lett. 5 (7) (2016) 805–808.
[20] Z. Ding, L. Yuan, G. Liang, A. Gu, Thermally resistant thermadapt shape memory crosslinked polymers based on silyl ether dynamic covalent linkages for self-folding and self-deployable smart 3D structures, J. Mater. Chem. A 7 (16) (2019) 9736–9747.
[21] J. Meng, Y. Zeng, P. Chen, J. Zhang, C. Yao, Z. Fang, K. Guo, New ultrastiff bio-furan epoxy networks with high Tg: Facile synthesis to excellent properties, Eur. Polym. J. 121 (2019) 109292.
[22] X. Wang, W. Guo, L. Song, Y. Hu, Intrinsically flame retardant bio-based epoxy thermosets: A review, Compos. Part B 179 (2019) 107487.
[23] J.-T. Miao, L. Yuan, Q. Guan, G. Liang, A. Gu, Biobased heat resistant epoxy resin with extremely high biomass content from 2,5-furandicarboxylic acid and eugenol, ACS Sustainable Chem. Eng. 5 (8) (2017) 7003–7011.
[24] V. Froidevaux, C. Negrell, S. Caillol, J.-P. Pascault, B. Boutevin, Biobased amines: from synthesis to polymers; present and future, Chem. Rev. 116 (22) (2016) 14181–14224.
[25] R. Auvergne, S. Caillol, G. David, B. Boutevin, J.-P. Pascault, Biobased thermosetting epoxy: present and future, Chem. Rev. 114 (2) (2014) 1082–1115.
[26] M.V. Maffini, B.S. Rubin, C. Sonnenschein, A.M. Soto, Endocrine disruptors and reproductive health: The case of bisphenol-A, Mol. Cell. Endocrinol. 254–255 (2006) 179–186.
[27] J. Dai, N. Teng, J. Liu, J. Feng, J. Zhu, X. Liu, Synthesis of bio-based fire-resistant epoxy without addition of flame retardant elements, Compos. Part B 179 (2019) 107523.
[28] D. Guzmán, X. Ramis, X. Fernández-Francos, S. De la Flor, A. Serra, New bio-based materials obtained by thiol-ene/thiol-epoxy dual curing click procedures from eugenol derivates, Eur. Polym. J. 93 (2017) 530–544.
[29] S. Aoyagi, T. Shimasaki, N. Teramoto, M. Shibata, Bio-based polymer networks by thiol-ene photopolymerization of allylated l-glutamic acids and l-tyrosines, Eur. Polym. J. 101 (2018) 151–158.
[30] Y. Tian, Q. Wang, K. Wang, M. Ke, Y. Hu, L. Shen, Q. Geng, J. Cheng, J. Zhang, From biomass resources to functional materials: A fluorescent thermosetting material based on resveratrol via thiol-ene click chemistry, Eur. Polym. J. 123 (2020) 109416.
[31] J.-T. Miao, L. Yuan, G. Liang, A. Gu, Biobased bismaleimide resins with high renewable carbon content, heat resistance and flame retardancy via a multi-functional phosphate from clove oil, Mater. Chem. Front. 3 (1) (2019) 78–85.
[32] A. Pellis, S. Weinberger, M. Gigli, G.M. Guebitz, T.J. Farmer, Enzymatic synthesis of biobased polyesters utilizing aromatic diols as the rigid component, Eur. Polym. J. 130 (2020) 109680.
[33] T. Liu, C. Hao, S. Zhang, X. Yang, L. Wang, J. Han, Y. Li, J. Xin, J. Zhang, A self-healable high glass transition temperature bioepoxy material based on vitrimer chemistry, Macromolecules 51 (15) (2018) 5577–5585.
[34] Z. Ma, Y. Wang, J. Zhu, J. Yu, Z. Hu, Bio-based epoxy vitrimers: Reprocessibility, controllable shape memory, and degradability, J. Polym. Sci. Part A Polym. Chem. 55 (10) (2017).
[35] S. Zhao, M.M. Abu-Omar, Recyclable and malleable epoxy thermoset bearing aromatic imine bonds, Macromolecules 51 (23) (2018) 9816–9824.
[36] X. Xu, S. Ma, J. Wu, J. Yang, B. Wang, S. Wang, Q. Li, J. Feng, S. You, J. Zhu, High-performance, command-degradable, antibacterial Schiff base epoxy thermosets: synthesis and properties, J. Mater. Chem. A 7 (25) (2019) 15420–15431.
[37] S. Wang, S. Ma, Q. Li, X. Xu, B. Wang, W. Yuan, S. Zhou, S. You, J. Zhu, Facile in situ preparation of high-performance epoxy vitrimer from renewable resources and its application in nondestructive recyclable carbon fiber composite, Green Chem. 21 (6) (2019) 1484–1497.
[38] J. Zhang, Z. Li, L. Zhang, J. García Molleja, D.-Y. Wang, Bimetallic metal-organic frameworks and graphene oxide nano-hybrids for enhanced fire retardant epoxy composites: A novel carbonization mechanism, Carbon 153 (2019) 407–416.
[39] J.-T. Miao, L. Yuan, Q. Guan, G. Liang, A. Gu, Biobased epoxy resin derived from eugenol with excellent integrated performance and high renewable carbon content, Polym. Int. 67 (9) (2018) 1194–1202.
[40] J.R. Mauck, S.K. Yadav, J.M. Sadler, J.J. La Scala, G.R. Palmese, K.M. Schmalbach, J.F. Stanzione, Preparation and characterization of highly bio-based epoxy amine thermosets derived from lignocellulosics, Macromol. Chem. Phys. 218 (14) (2017) 1700013.
[41] W.C. Oliver, G.M. Pharr, An improved technique for determining hardness and elastic modulus using load and displacement sensing indentation experiments, J Mater. Res. 7 (6) (1992) 1564–1583.
[42] X. Yang, L. Guo, X. Xu, S. Shang, H. Liu, A fully bio-based epoxy vitrimer: Self-healing, triple-shape memory and reprocessing triggered by dynamic covalent bond exchange, Mater. Des. 186 (2020) 108248.
[43] S. Zhang, T. Liu, C. Hao, L. Wang, J. Han, H. Liu, J. Zhang, Preparation of a lignin-based vitrimer material and its potential use for recoverable adhesives, Green Chem. 20 (13) (2018) 2995–3000.
[44] M. Ozawa, M. Shibata, Reprocessable bismaleimide-diamine thermosets based on disulfide bonds, React. Funct. Polym. 146 (2020) 104404.